Materials Transactions, Vol. 61, No. 3 (2020) pp. 430 to 437

Ductility Improvement Mechanism of Ti–6Al–4V+O Sintered Material[*1]

Kento Kamiyama[1,*2], Shota Kariya[1,*2], Mizuki Fukuo[1,*2], Junko Umeda[2] and Katsuyoshi Kondoh[2,*3]

[1]*Department of Mechanical Engineering, Graduate School of Engineering, Osaka University, Suita 565-0871, Japan*
[2]*Joining and Welding Research Institute Osaka University, Ibaraki 567-0047, Japan*

The previous study indicated powder metallurgy (PM) Ti-64 alloys with oxygen showed the increment of not only their tensile strength but elongation. This study investigated the elongation improvement mechanism of Ti-64 alloys with oxygen atoms. The mix of Ti-64 alloy powder and TiO_2 particles (0∼0.4 mass%) was used as starting materials and consolidated by spark plasma sintering (SPS). The following heat treatment in vacuum was applied to sintered materials. β transus temperature increased by oxygen addition because it was one of α-phase stabilizer elements. Prior-β grains size and aspect ratio of α-Ti grains were changed by heat treatment conditions. For example, Ti-64+O alloys after heat-treated at β-phase temperature range showed acicular α-Ti grains with a large aspect ratio (6.1∼7.0) although those with heat treatment at $\alpha+\beta$-phase temperature had α-grains with a small aspect ratio of 3.3∼4.0. These grain morphology changes strongly depended on the temperature of heat treatment, not oxygen contents. In addition, the latter materials indicated high elongation (16∼17%) compared to the former with 9∼10%. When Ti-64+O alloy specimens after tensile test were analyzed by SEM-EBSD, Kernel average misorientation (KAM) maps showed many plastic strains induced in small aspect ratio α-Ti grains. [doi:10.2320/matertrans.Y-M2019869]

(Received November 13, 2019; Accepted December 4, 2019; Published January 31, 2020)

Keywords: *titanium alloy, oxygen, powder metallurgy, phase transformation, ductility*

1. Introduction

Ti–6Al–4V alloys are widely used in the aircraft parts and biomedical equipment because of their excellent properties such as high strength, ductility and corrosion resistance. They contain 6 mass% aluminum (Al), and 4 mass% vanadium (V). These elements serve to stabilize α and β phases of titanium, respectively. This is one of the $\alpha+\beta$ type titanium alloys where both α and β phases co-exist even at room temperature.

Strengthening and ductility improvement of this alloy has been well investigated. Among the previous studies, it has been reported that strength of titanium and its alloys can be significantly increased by solid solution behavior with the elements abundant on the Earth (i.e. ubiquitous alloying elements).[1,2] Titanium alloys exhibit a remarkable improvement in strength even with small additions of oxygen, an interstitial solid solution element in Ti. Although the elongation to failure decreases with increasing the oxygen addition, it has been confirmed that this effect approaches a limit at approximately 0.1 mass% O content.[3] In our previous experiment, the mechanical properties of oxygen-soluted Ti–6Al–4V extruded materials were evaluated. Specimens were prepared by adding 0 to 1.0 mass% of titanium dioxide (TiO_2) particles to Ti–6Al–4V alloy powder. The elongation to failure was evaluated to be 16.5% and 23.3% for the 0 mass% and 0.5 mass% TiO_2 specimens, respectively. This suggest that small amounts of added oxygen can improve the strength while maintaining sufficient ductility. The solution for the ductility improvement mechanism leads to not only the weight reduction of products by high strengthening but the improvement of their reliability and formability, and results in a remarkable contribution of the titanium materials industries.

This study investigates the mechanisms of ductility improvement of Ti–6Al–4V alloys with oxygen solid solution. As microscopic structure changes of the material, the crystal lattice strain was induced by soluted atoms. In terms of macroscopic structure, the grain morphology changes due to modified phase transformation behavior. Both have been considered in this study.

2. Experimental Procedure

In this study, pre-alloyed Ti–6Al–4V powder (TILOP-64-45, Osaka Titanium Technologies Co., Ltd.) and TiO_2 particles (purity 99.5%, Kishida Science Co., Ltd.) were used as starting materials. The morphology of the initial Ti–6Al–4V powder was spherical (Fig. 1). A Laser Diffraction Particle Size Distribution Analyzer (LA-950, HORIBA, Ltd.) was used to determine the particle size and distribution. The average particle diameters of Ti–6Al–4V and TiO_2 were 24.9 μm and 3.48 μm respectively. Before mixing these powders, a naphthenic oil (Crisef-oil H8, JXTG Energy Co.,

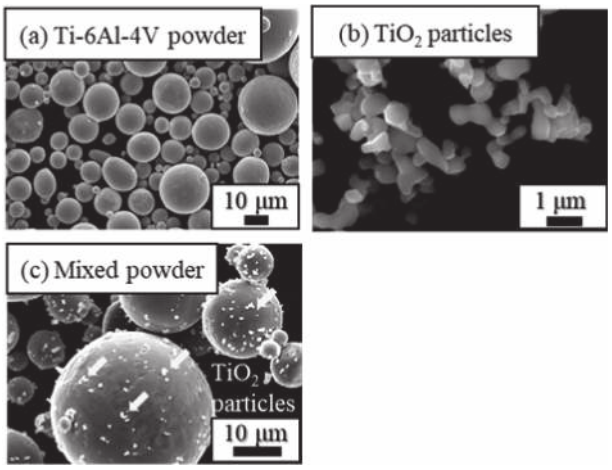

Fig. 1 SEM observation images of raw powders used in this study. (a) Ti–6Al–4V alloy powder, (b) TiO_2 particles and (c) elemental mixture of Ti–6Al–4V+TiO_2 powder (0.4 mass%TiO_2).

[*1]This Paper was Originally Published in Japanese in J. Jpn. Soc. Powder Powder Metallurgy **65** (2018) 699–706.
[*2]Graduate Student, Osaka University
[*3]Corresponding author, E-mail: kondoh@jwri.osaka-u.ac.jp

Ltd.) was added at a mass ratio of 0.025% to a predetermined amount of Ti–6Al–4V alloy powder. This was sealed in a plastic bottle and placed on a small ball mill rotating stand (AV-1 type, manufactured by Asahi Rika Manufacturing Co., Ltd.) to mix for 3.6 ks at 90 rpm under atmospheric condition. Afterwards, TiO_2 particles were added into Ti–6Al–4V powder at a predetermined mixing ratios (0 to 0.6 mass%) and mixed at a frequency of 60 Hz for 10.8 ks using a rocking mill (RM - 05, Seiwa Giken Co., Ltd.). In order to distribute TiO_2 particles uniformly, 100 g of zirconia (ZrO_2) media balls ($d = 10$ mm) were added before mixing. Figure 1(c) shows the morphology of mixed powder with added 0.4 mass% TiO_2 particles. After mixing, it was confirmed that the TiO_2 particles were dispersed uniformly on the surface of the Ti–6Al–4V alloy powder.

The mixed powder was sintered at 1373 K for 7.2 ks at 30 MPa pressure under vacuum condition (6 Pa) by a spark plasma sintering method (SPS). After sintering, specimens were furnace cooled.

For further homogenization of the solid solution state of oxygen atoms in Ti–6Al–4V matrix, heat treatment was performed using a vacuum furnace (FT-1200R-250, FULL-TECH FURNACE CO., Ltd.) with following parameters; 100 Pa vacuum, 20 K/min heating rate and 10.8 ks. The holding temperature was set at 1223, 1273 and 1373 K to investigate the relationship between the oxygen addition amount and phase region during heat treatment. After heat treatment, specimens were furnace cooled in the furnace. In order to confirm the existence form of α phase and β phase during heat treatment, water-quenched specimens from the three holding temperatures were also prepared.

For microstructural studies, specimens were first ground using abrasive papers from #80 to #4000. Specimens surfaces were subsequently polished using an alumina solution (Master Prep Polishing Suspension 0.05 Micron, Buhler ITW Japan Co., Ltd.). After polishing, chemical etching treatment was performed for microstructure observation using a titanium corroding solution (H_2O:HF:HNO_3 = 100:1:5). The microstructures were observed with a scanning electron microscope (SEM, JSM-7100F, JEOL Ltd.).

Micrographs obtained by the backscattered electron images of the scanning electron microscope were copied on paper in order to measure the average length and thickness of α grains. Tracing paper was laid over the backscattered electron images and the grain boundaries were scanned. The longest and shortest dimensional lengths of multiple grains were calculated using the image processing software (Image Pro Plus 4.0J) and the short length was considered as the thickness of each grain. The aspect ratios of the grains were calculated by dividing the length by the thickness. For data reliability, shortest and longest dimensional lengths were measured for more than 1000 grains, and an average grain length and thickness was determined.

X-ray diffraction (XRD) analyses were also performed to identify phases and confirm the formation of a solid solution. The different lattice constants between specimens, due to varying oxygen solute content, was quantitatively evaluated. The lattice constants of the a and c axes in Ti crystal with α phase (hcp structure) were calculated from the diffraction pattern obtained by the X-ray Diffractometer (XRD-6100, Shimadzu Corporation). For measurement, a Cu-Kα ray (λ = 1.5418 Å) was used with following parameters: tube voltage; 40.0 kV, tube current; 30.0 mA, DS, SS; 1°, RS; 0.3 mm, scan rate; 1.0°/min.

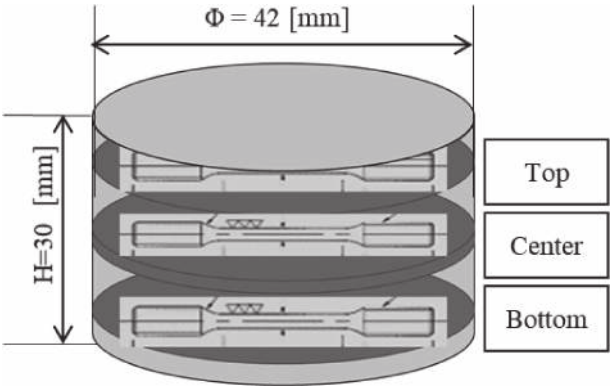

Fig. 2 Illustration of sampling method of tensile specimen machined from sintered Ti–6Al–4V+TiO_2 material.

To analyze the fraction ratio and distribution of α and β phases in Ti–6Al–4V and the crystal orientation, an electron backscatter diffraction (EBSD) analysis was performed. The EBSD pattern was detected with a high-speed and high-sensitivity CCD camera (Digi View IV Detector, TSL Solutions Co., Ltd.) mounted on a SEM (JSM-6500F, JEOL Ltd.). Application software (TSL OIM Data Collection 5.31, TSL Solutions Co., Ltd.) was used to analyze grain orientation and strain.

In order to evaluate the mechanical properties, a tensile test was performed by the tensile tester (Autograph AG-X 50 kN, Shimadzu Corporation). Tensile specimen preparation is shown in Fig. 2. Three tensile specimens were machined from sintered materials. Tensile specimens with a diameter of 3 mm and gauge length of 10 mm were used. A screw type was adopted for fixing the test piece to the testing machine jig. The test was carried out at a strain rate of 5.0×10^{-4}/s at room temperature. The strain was recorded by measuring the position of reference markings using a CCD camera (DVE-101, Shimadzu Corporation) attached to the tensile tester.

3. Results and Discussions

3.1 Effect of oxygen addition dissolved from TiO_2 particles on Ti matrix

The quantitative analysis was performed to confirm both the original oxygen and nitrogen contents of the Ti–6Al–4V alloy powder and their increased contents of the Ti–6Al–4V alloy powder caused by addition of TiO_2 particles (0 to 0.4 mass%). The results are presented in Table 1. Oxygen was also detected in the sintered material without TiO_2 particles (0 mass% TiO_2). This is likely to have originated from the surface oxide film of the Ti–6Al–4V alloy powder. Nitrogen is also known to affect the ductility of titanium.[3,4] However, as shown in Table 1, the nitrogen content was 0.02 to 0.03 mass% regardless of the amount of the added TiO_2 particles. Both specimens satisfy <0.05 mass% N requirement of the Japanese Industrial Standards (JIS).[5] Due to the negligible nitrogen content from TiO_2 particles addition, it had little effect on mechanical properties and microstructures.

Table 1 Oxygen and nitrogen contents of sintered Ti–6Al–4V+TiO_2 powder materials with different TiO_2 contents.

	Oxygen content [mass%]	Nitrogen content [mass%]
Ti-6Al-4V raw powder	0.15	0.01
0 mass%TiO_2	0.21	0.02
0.2 mass%TiO_2	0.30	0.02
0.4 mass%TiO_2	0.36	0.03

It is known that oxygen atoms are dissociated from TiO_2 particles by thermal decomposition during sintering.[2] The diffusion of oxygen atoms into the titanium was investigated. It is expected that oxygen atoms thermally decompose from TiO_2 particles during the sintering process and diffuse into the Ti matrix. This is due to the difference in oxygen concentration between the TiO_2 particles and the Ti matrix. The crystal lattice of Ti is deformed as a result of soluted oxygen. This deformation behavior can be quantitatively evaluated from the peak shift amount of XRD patterns.[6] Therefore, XRD analysis was applied to evaluate of the lattice constant changes in the Ti crystal which resulted from the oxygen solid solutioning. The previous studies have attributed the significant increase in the lattice constant of the c-axis due to the solid solution of oxygen atoms in α-Ti. While the a-axis lattice constant increase was 0.7×10^{-3} Å, that of the c-axis was 4.0×10^{-3} Å.[7] XRD scanning was performed in the range of $2\theta = 70°$ to 80°. The peaks around $2\theta = 71.0°$ (Fig. 3(a), (103)) and 76.8° (Fig. 3(b), (112)) indicating α phase were investigated. When increasing the amount of TiO_2 additives, a shift of α phase diffraction peak at $2\theta = 71.0°$ and 76.8° towards lower angles was observed. This indicates the lattice constant increased with increase of oxygen in the solid solution. The lattice constants of a-axis and c-axis of α phase crystal were calculated using Bragg's law and the obtained diffraction peak positions. The results showed that their increase rates were 0.1×10^{-3} Å/at%O and 5.0 × 10–3 Å/at%O in the a-axis and c-axis directions, respectively. The value in the c-axis direction is remarkably large compared with that of the a-axis direction due to the oxygen solid solutioning. This result agrees well with the previous study.[7]

The structural change of β phase due to the difference in the oxygen content is shown in Fig. 3(c). The diffraction peak at $2\theta = 39.6°$ shifted to the lower angle, indicating an enlargement of the (110) plane. The lattice constant of a-axis in β phase was increased by 4.5×10^{-3} Å per 1 at% oxygen. Though oxygen is an α phase stabilizing element, it has been reported that oxygen atoms are dissolved in β phase to an upper limit of about 2 at%.[8] Since the maximum amount of added oxygen in this study was 0.71 at% and β phase diffraction peaks were shifted, oxygen atoms were dissolved in β phase.

3.2 Changes in crystal structure by the oxygen solid solutioning

Figure 4 shows the structure observation results (back-scattered electron images) when 0∼0.4 mass% TiO_2 particles were added. In the 0 mass% TiO_2 material (Fig. 4(a)), the acicular α grains were dominant, but in the material with the 0.2 and 0.4 mass% TiO_2 (Fig. 4(b) and (c)), the morphology of α grains was close to the equiaxed shape. As marked by the arrows, each material was divided by α grains with a large aspect ratio. The size of the divisions was significantly different between TiO_2 non-added and added. Therefore, the IQ and IPF maps from the EBSD of these specimens were analyzed. In the IPF map, β phases located inside α phase with large aspect ratio had the same crystal orientation. From this result, they are considered as an evolved single β grain during heat treatment. Hereafter, these aggregates of β phases are referred to as prior β grains. In the 0 mass% TiO_2 material, many prior β grains greater than 500 μm in size were found, while the 0.4 mass% TiO_2 additives had a grain size of about 200 μm. Hence, it was confirmed that the

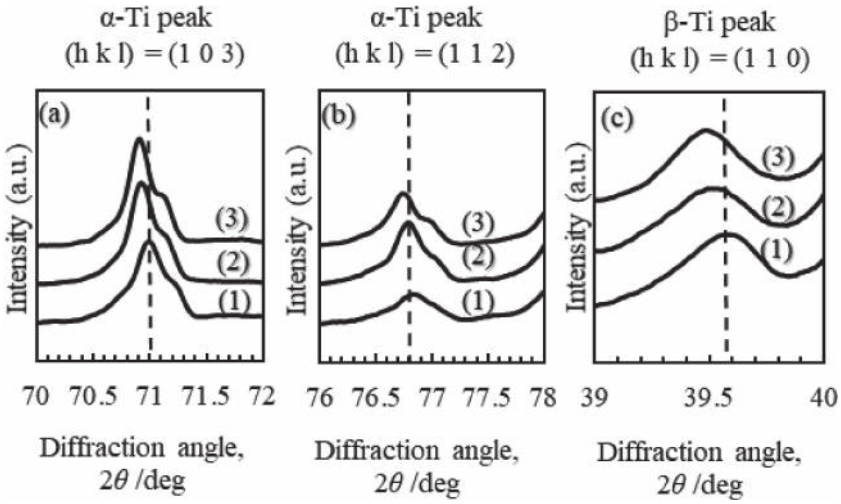

Fig. 3 XRD profiles of sintered Ti–6Al–4V+TiO_2 powder materials: Diffraction angle $2\theta = 70∼72°$ (a), $2\theta = 76∼78°$ (b) and $2\theta = 39∼40°$ (c): TiO_2 additional content of 0 mass% (1), 0.2 mass% (2) and 0.4 mass% (3).

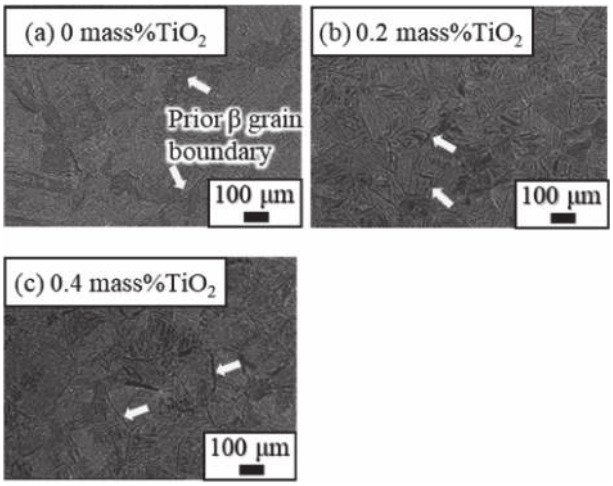

Fig. 4 SEM observation images of sintered Ti–6Al–4V+TiO_2 materials: TiO_2 additional content of 0 mass% (a), 0.2 mass% (b) and 0.4 mass% (c).

size of the prior β grain changes remarkably depended on the amount of soluted oxygen atoms.

3.3 Correlation between heat treatment temperature and structure change of Ti

Since oxygen is an α phase stabilizing element, the β transus temperature rises with increase in the amount of oxygen content.[9] Figure 5 shows the relation between oxygen content and the β transus temperature (T_β) in Ti–6Al–4V alloy,[9] which was obtained from the following equation.

$$T_\beta = 937 + 243 \times \text{Oxygen (mass\%)} \qquad (3.1)$$

Here, T_β was calculated by substituting the oxygen content according to the quantitative analysis shown in Table 1. In the 0 mass% TiO_2 material, T_β was 1257 K, in contrast when 0.2 and 0.4 mass% TiO_2 was added, T_β increased to 1282 K and 1297 K, respectively. Since 1273 K was selected as the heat treatment temperature in this study, the 0 mass% TiO_2 material consisted of the single β phase, whereas the materials containing 0.2 and 0.4 mass% TiO_2 showed $\alpha+\beta$ phases during heat treatment.

Therefore, the factors which contribute to form microstructure were identifiable by controlling the heat treatment temperature T_h. The relationship between the heat treatment temperature T_h and the change in microstructure was also investigated. From Fig. 5, the heat treatment temperature was set to $T_h = 1223$ K where both the 0 and 0.4 mass% TiO_2 specimens were in the $\alpha+\beta$ region and $T_h = 1373$ K where both specimens were in the single β phase region. The results of microstructure observation are shown in Fig. 6. In the specimens with heat treatment at 1373 K (in the single β phase region), many acicular α grains with large aspect ratios were detected. On the other hand, in the specimens heat-treated at 1223 K (in the $\alpha+\beta$ region), nearly equiaxed α grains were detected. It was also confirmed that the heat treatment in the single β phase region produced larger primary β grains than heat treatment in the $\alpha+\beta$ region. The grain size measurement of the primary β grains is shown in Table 2. While the average grain size of prior β grains in specimens heat-treated in the 2-phase area was between 170 μm and 230 μm, prior β grains in the specimen heat-treated in the single β phase area became coarse grains exceeding 500 μm. From these results, it was concluded that the microstructures changed depending on the phase region in the heat treatment. Coarse primary β grains and acicular α grains were found in the specimens heat-treated at the temperature range above the β transus. Numerous equiaxed α

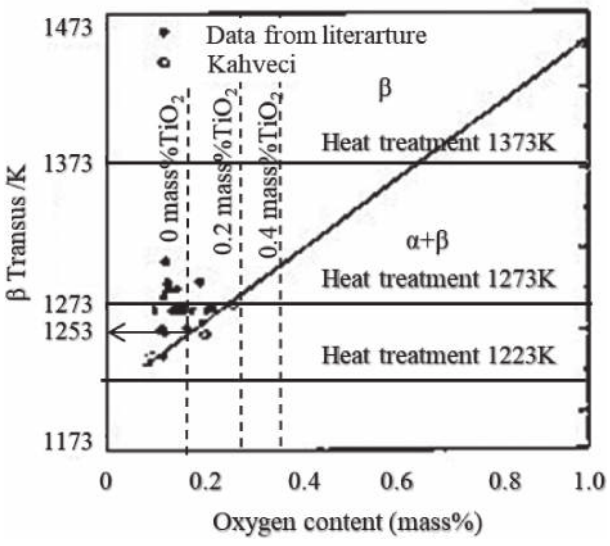

Fig. 5 β transus temperature of Ti–6Al–4V alloys as a function of oxygen content.[9]

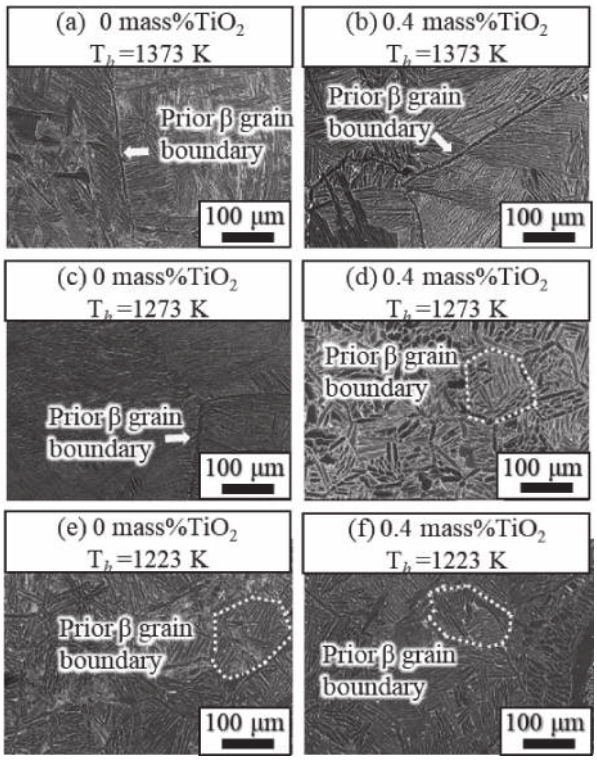

Fig. 6 SEM observation images of sintered Ti–6Al–4V+TiO_2 materials. 0 mass%TiO_2 $T_h = 1373$ K (a), 0.4 mass%TiO_2 $T_h = 1373$ K (b) 0 mass%TiO_2 $T_h = 1273$ K (c), 0.4 mass%TiO_2 $T_h = 1273$ K (d) 0 mass%TiO_2 $T_h = 1223$ K (e) and 0.4 mass%TiO_2 $T_h = 1223$ K (f).

Table 2 Mean grain size of prior β grains of sintered Ti–6Al–4V+TiO_2 materials with different temperatures of heat treatment (T_h): 1373 K, 1273 K and 1223 K.

Temperature of heat treatment, T_h/ K	0 mass%TiO_2 /μm	0.4 mass%TiO_2 /μm
1373	> 500	> 500
1273	> 500	172
1223	223	230

grains were observed in the specimens heat-treated at the 2 phase $\alpha+\beta$ stable temperature. Hereinafter, the specimens heat-treated at single β phase temperature are classified as Group I, and those at the 2 phase $\alpha+\beta$ temperature were classified as Group II.

The formation mechanism of crystal structures in Group I and Group II was discussed. By water-quenching treatment, the residual α phases at the heat treatment temperature should remain as α phase at room temperature while β phase transforms into martensite phase (α').[10] The evolution of α and β phases during heat treatment was investigated using the water-quenched materials. Group I (with 0 mass% TiO_2 additive) and Group II (with 0.4 mass% TiO_2 additive) materials were water-quenched from 1373 K and 1273 K, respectively. The EBSD results showed that the Group I material contained only α' phases. Therefore, it was assumed that the specimen was fully β phase during heat treatment. On the other hand, the Group II contained both α' and α phases. This suggests that both α and β phases exist during heat treatment.

Figure 7 indicates α and β grains formation mechanism during cooling after heat treatment, as inferred from the results. In the case of Group I, at the higher temperature than the β transus, all of the α phases transformed into β phase, and β grain growth occurred at high temperature. After the homogenizing treatment, the temperature gradually decreased by cooling and shifts from the single β phase region to the $\alpha+\beta$ region. α grain formation starts at the grain boundaries of the β phase.[11] As cooling progresses, α grains transform within the β phase.[12] During this $\beta \rightarrow \alpha$ phase transformation, α phase grows according to the orientation relationship of Burgers vectors[10] shown below.

$$\{110\}_\beta \parallel (0002)_\alpha \quad (3.2a)$$

$$[111]_\beta \parallel [11\bar{2}0]_\alpha \quad (3.2b)$$

α grains in β phases grow preferentially according to coarse prior β phase crystal orientation until encountering other α grains with a different orientation. As a result, α grains formed relatively large acicular crystals.

In Group II, the transformation from α phases to β phases also proceeded with the increasing temperature. Since the specimen was held at 2 phase $\alpha+\beta$ stable temperature, α grains also presented in the heat treatment process, which leads to the suppressed β phases growth. After the heat treatment process, as the temperature decreases, α phase is transformed according to the relationship of the orientation within β phase. However, the grain boundaries of the residual α phase amongst β grains obstruct the growth of acicular α grains generated after the $\beta \rightarrow \alpha$ phase transformation.

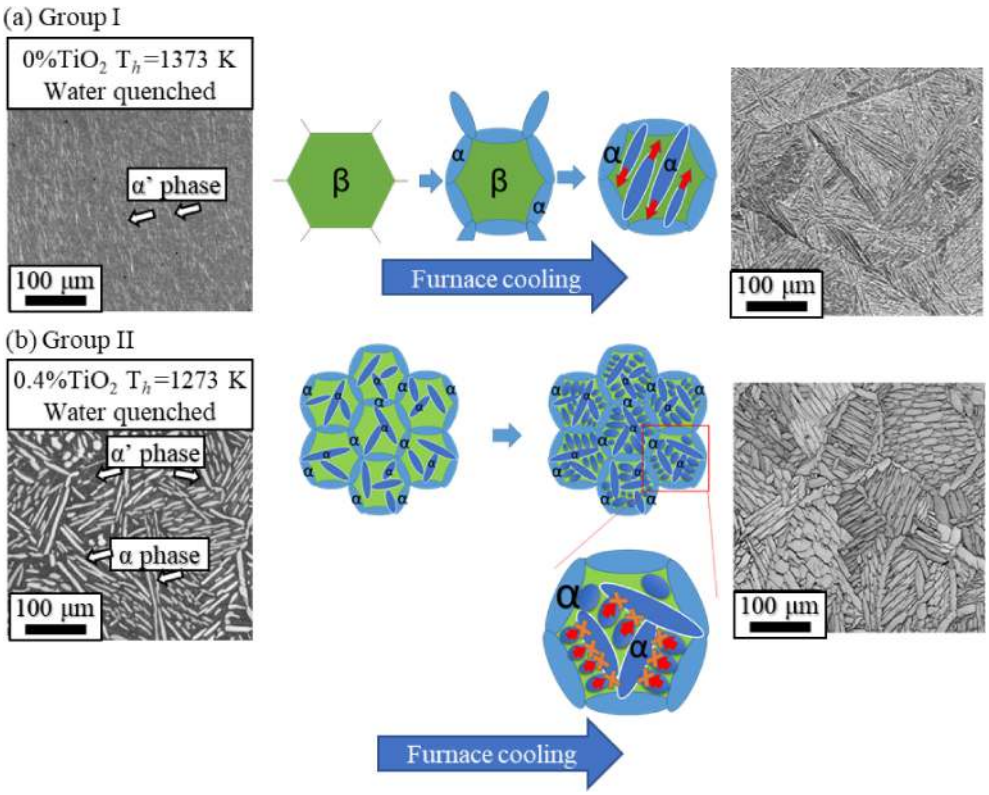

Fig. 7 Illustration of deformation mechanism of $\beta \rightarrow \alpha + \beta$ transformation in Ti–6Al–4V (Group I (a) and Group II (b)).

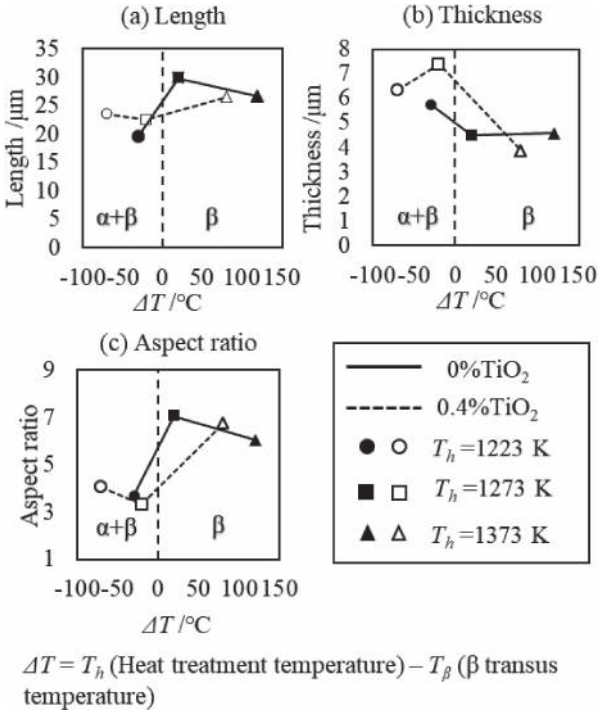

Fig. 8 Dependence of ΔT ($= T_h - T_\beta$) on length (a), thickness (b) and aspect ratio (c) of α phase.

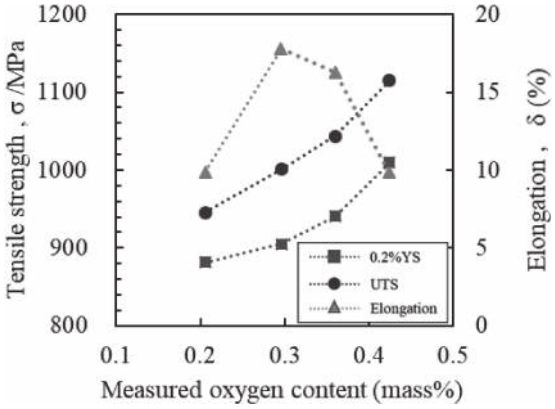

Fig. 9 Dependence of tensile properties of Ti–6Al–4V+TiO_2 sintered materials on measured oxygen content.

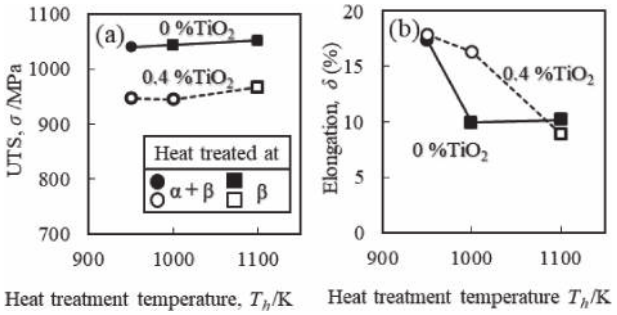

Fig. 10 Dependence of tensile properties of Ti–6Al–4V+TiO_2 sintered materials on the temperature of heat treatment (a) UTS and (b) Elongation.

Hence, the aspect ratio of the formed α grains was smaller, and relatively fine crystal grains were formed.

It was found that the heat treatment affected the morphology of α grains significantly. The relationship between the phase region during heat treatment and α grains morphology has been summarized in Fig. 8. The horizontal axis represents the difference ΔT ($= T_h - T_\beta$) between the heat treatment temperature T_h and phase transformation point T_β. The vertical axis represents (a) the length, (b) the thickness and (c) the aspect ratio of α grains. The α grains were 19 to 23 μm in length for Group II specimens, and an increased 26 to 30 μm for the Group I specimens. The thickness of α grains was approximately 5.8 to 7.3 μm for the Group II specimens, and approximately 3.8 to 4.4 μm for the Group I specimens. The aspect ratio of α grains ranged from 6.1 to 7.0 for the Group I specimens, and a lower range of 3.3 to 4.0 in the Group II specimens. They agree with the mechanism of grain growth as shown in the schematic diagram in Fig. 7.

3.4 Mechanical properties of Ti–6Al–4V sintered alloy with oxygen solution

The tensile properties results of Ti–6Al–4V sintered alloys with different oxygen contents are discussed. The correlation between the ductile behavior and the crystal structure changes was investigated based on the microstructures analysis result shown in the section 3.3. The tensile test results of the specimen heat-treated at 1273 K are presented in Fig. 9. The tensile strength (UTS) and the yield strength (0.2%YS) were increased remarkably with the increased oxygen content. The 0.2%YS and UTS of the 0 mass% TiO_2 (0.21 mass% O) specimen was 881 MPa and 945 MPa, respectively. For the 0.6 mass% TiO_2 (0.36 mass% O) specimen, 0.2% YS and UTS was measured to be 1010 MPa and 1115 MPa, respectively. The elongation to failure was 9.8% in the 0 mass% TiO_2 specimen, 17.8% in the 0.2 mass% TiO_2 specimen (0.30 mass% O), and 16.3% in the 0.4 mass% TiO_2 specimen (0.36 mass% O). The specimens with TiO_2 have higher elongation to failure than that of the non-added TiO_2 specimen.

In order to investigate the effect of the heat treatment temperature on the mechanical properties, tensile testing was conducted on the specimens prepared at the different heat treatment temperatures ($T_h = 1223$, 1373 K) discussed in the previous section. By presenting the difference ΔT ($= T_h - T_\beta$) between the heat treatment temperature T_h and phase transformation point T_β on the horizontal axis, the relationship between phase area during heat treatment and the tensile strength characteristics was charted and presented in Fig. 10. As for tensile strength (a), the 0.2% YS was in the range of 810 to 881 MPa and the UTS was about 875 to 967 MPa in the 0 mass% TiO_2 specimen. In the 0.4 mass% TiO_2 specimen, with increased oxygen solid solution amount, the strength values were as follows: 0.2%YS between 894 MPa and 940 MPa, and UTS between 960 MPa and 1043 MPa. Meanwhile, in the specimen with the same oxygen solid solution amount, there was no strong correlation between the specimens with acicular α (Group I) and with equiaxed α grains (Group II). Therefore, in the temperature range of the heat treatment examined in this study, the tensile strength of these specimens was dependent on the amount of oxygen dissolved in α and β phase rather than microstructures. On the other hand, a strong dependence of

the elongation to failure on a phase morphology during heat treatment was clarified. The elongation to failure was 16 to 18% for the Group II specimens and 5 to 10% for the Group I specimens. Its value of the Group I specimens was relatively lower than that of the Group II, even considering their scatters.

3.5 Mechanism of ductility improvement

The high ductility improvement mechanisms are discussed based on the relationship between elongation values and aspect ratio of α grains. The relationship between the elongation at fracture and the aspect ratio of α grains was analyzed as shown in Fig. 11. Though the specimens with aspect ratios of 3 to 4 were associated with elongation to failure values of 16 to 18%, the specimens with the aspect ratios of 6 or more showed 5 to 10% elongations. Thus, a strong correlation was observed between the aspect ratio of α grains and the elongation.

Plastic deformation generated in the tensile test process is caused by dislocation motion and slip. The microstructures with a large amount of strain are able to exhibit high ductility. It has also been reported that specimens with large grain deformations have a higher elongation because of its high plastic deformability.[13] As shown in Fig. 11, the specimens with a low aspect ratio α grains had higher elongation values. The residual strain distribution in the specimen after the tensile test was analyzed. At the same time, the relationship between the shape of α grains and the strain distribution were investigated. The strain distribution can be observed in the KAM (Kernel Average Misorientation) map calculated by the difference in crystal orientation between adjacent measurement points in the EBSD analysis. The yellow areas indicate large accumulated strains. The KAM analysis results before and after the tensile test of the 0 mass% TiO_2 and the 0.4 mass% TiO_2 additive are shown in Fig. 12 along with the IQ maps. Though small amounts of strain can be observed at the prior β grain boundaries from the KAM map before the tensile test (-1), the strain amount increased significantly in almost all areas after the tensile test (-2). In the KAM maps after the tensile test of the 0 mass% TiO_2 specimen (a-2), the strain mainly occurred in the vicinity of the α phase grain boundary, and hardly observed within the grains. On the other hand, large amount of strain was introduced not only in the grain boundaries but also within small aspect ratio grains in the 0.4 mass% TiO_2 additive (b-2). Therefore, it can be considered that strains tend to be accumulated in the grains with small aspect ratios, as compared with α grains with large aspect ratios. From the above discussions, it is concluded that the deformability of α grains with a small aspect ratio is larger compared to the acicular α grains. Hence, in tensile deformation, the specimens comprised of acicular α grains (Group I) ruptured from small fracture strains. Alternatively, the specimens containing a large amount of equiaxed α grains (Group II) were easily deformed and exhibited a high elongation value because of a high deformability of these equiaxed α grains.

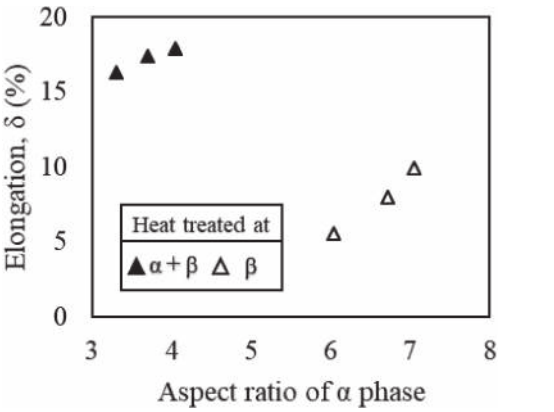

Fig. 11 Dependence of elongation on aspect ratio of α phase of Ti–6Al–4V+TiO_2 sintered materials.

4. Conclusion

(1) It has been confirmed that the morphologies of the microstructures in the Ti–6Al–4V sintered alloy were

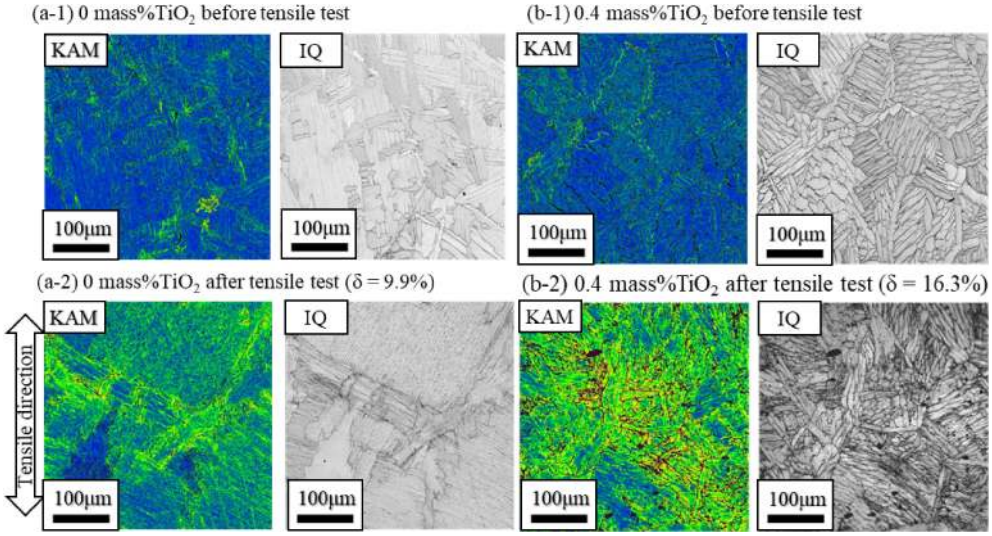

Fig. 12 Kernel Average Misorientation (KAM) maps and Image Quality maps of sintered Ti–6Al–4V + 0 mass%TiO_2 (a) and 0.4 mass%TiO_2 (b) materials: Before tensile test (-1) and after tensile test (-2).

greatly changed due to phase transformations during the cooling process and the difference in phase region during the heat treatment. When heat treatment was performed in the single β phase, many acicular α grains were formed within coarse and large β grains with the size of 500 μm or more. In contrast, in the heat treatment in the $\alpha+\beta$ region, the particle diameter of prior β grains was between 170 μm and 230 μm, and nearly equiaxed α grains were observed.

(2) In regard to the formation mechanism of the different microstructures, when the heat treatment at the single β phase was applied, α grains grew preferentially until they come into contact with other phases with different orientations in accordance with the coarse crystal orientation of the prior β grain. As a result, acicular α grains with a large aspect ratio were formed. Meanwhile, in case of the heat treatment in the $\alpha+\beta$ region, since β grains were small, α grains in prior β grain boundaries were also small. Furthermore, α grain growth was interrupted by the residual α phase in the β phase, and therefore, the aspect ratios of α grains were small and relatively fine equiaxed α grains were formed.

(3) Specimens of 0 and 0.4 mass%TiO_2 content with different α grain aspect ratios were prepared by changing the heat treatment temperatures, and the strain distributions were analyzed before and after the tensile test. Much strain was accumulated within equiaxed α grains compared to the acicular α grains. Thus, it was considered that equiaxed α grains had a high deformability, causing a high ductility of sintered Ti alloys with equiaxed α grains.

Acknowledgments

This work was partially supported by the Japan Science and Technology Agency (JST) under Industry–Academia Collaborative R&D Program “Heterogeneous Structure Control: Towards Innovative Development of Metallic Structural Materials and the Amada Foundation under Research & Development Grant B (AF-2016003).

REFERENCES

1) T. Jones, K. Kondoh, T. Mimoto, N. Nakanishi and J. Umeda: Key Eng. Mater. **551** (2013) 118–126.
2) B. Sun, S. Li, H. Imai, T. Mimoto, J. Umeda and K. Kondoh: J. Smart Process. **1** (2012) 283–287.
3) M.J. Donachie: *Titanium: A Technical Guide*, 2nd edition, (ASM International, Almere, 2000) p. 27.
4) K. Kondoh, B. Sun, S. Li, H. Imai and J. Umeda: Int. J. Powder Metallurg. **50** (2014) 35–40.
5) Japanese Industrial Standards: JIS H 4650, (2012) 4.
6) Y. Waseda and E. Matsubara: *X Ray Structural Analysis*, 1st edition, (Uchida-roukakuho, Tokyo, 1998) pp. 40–41.
7) R. Montanari, G. Costanza, M.E. Tata and C. Testani: Mater. Charact. **59** (2008) 334–337.
8) T. Okabe, R. Suzuki, T. Oishi and K. Ono: Mater. Trans. **32** (1991) 485–488.
9) R. Boyer, E.W. Collings and G. Welsch: *Materials Properties Handbook Titanium Alloys*, 1st edition, (ASM International, Almere, 1994) p. 490.
10) T. Ahmed and H.J. Rack: Mater. Sci. Eng. A **243** (1998) 206–211.
11) E. Wielewski, D.B. Menasche, P.G. Callahan and R.M. Suter: J. Appl. Crystallogr. **48** (2015) 1165–1171.
12) G. Lutjering: Mater. Sci. Eng. A **243** (1998) 32–45.
13) S. Hashimoto, T. Tsuchiyama and S. Takaki: Tetsu-to-Hagané **103** (2017) 636–645.